Structural Study of Poly-Molybdate Ions in Acid Mo-Ni Aqueous Solutions

Kozo Shinoda, Eiichiro Matsubara[a], Masatoshi Saito, Yoshio Waseda, Tetsuji Hirato[a], and Yasuhiro Awakura[a]

Institute for Advanced Materials Processing, Tohoku University, Aoba-ku Sendai 980-77, Japan
[a] Department of Materials Science and Engineering, Graduate School, Kyoto University, Kyoto 606-01, Japan

Z. Naturforsch. **52 a,** 855–862 (1997); received November 10, 1997

The atomic structure of poly-molybdate ions formed in acid Ni-Mo aqueous solutions has been determined by applying anomalous X-ray scattering (AXS) and EXAFS methods. In a solution containing only molybdenum ions, we found only a poly-molybdate ion consisting of seven edge-sharing MoO_6 octahedra. In a solution containing both Mo and Ni ions, there exists another poly-molybdate ion consisting of 6 edge-sharing MoO_6 surrounding an Ni ion. The total coordination number of Mo and Ni ions around a molybdenum ion is reduced by half when introducing citric ions into the Ni and Mo solution. This indicates that the large poly-molybdate ion is decomposed to smaller molybdate ions when forming citric complexes. Since molybdenum-nickel alloys can not be electrodeposited from solutions without citric ions, we propose a view that the structural change of the poly-molybdate ions in the solutions is closely related with the mechanism of induced codeposition of molybdenum and nickel alloy. The results of small-angle X-ray scattering (SAXS) measurements also support this conclusion.

Key words: Anomalous X-ray Scattering, EXAFS, Mo-Ni Alloy Electroplating, Aqueous Solution, Poly-molybdate Ion.

1. Introduction

Electrodeposited molybdenum or tungsten amorphous alloys, such as Mo-Ni [1] and W-Co [2], provide superior corrosion and wear resistance. The catalytic activity of these alloys in the industrial production of hydrogen from alkaline-water electrolytic cells is also notable [3]. In addition to this practical relevance, the electrodeposition of molybdenum and tungsten alloys is of considerable interest. Pure molybdenum or tungsten can not be electrodeposited from an aqueous solution. It can only be electrically codeposited from an aqueous solution containing an iron-group metal. Brenner [4] described the electrodeposition of these alloys as induced codeposition. Several theoretical assumptions [5 - 9] have been made to explain the mechanism of induced codeposition. The electroplating conditions [2, 8 - 10], mechanical and chemical properties [11 - 13], atomic or micrographic structures [3,14] of the codeposited molybdenum or tungsten alloy have been intensively studied. However no experimental information is available about the environmental structure around a molybdenum ion and an iron-group metallic ion in aqueous solution. This prompted us to determine the atomic scale structure of molybdenum and nickel ions in the Mo-Ni aqueous solutions by EXAFS and anomalous X-ray scattering (hereafter, it is called AXS) methods. This will provide a new view in the study of induced codeposition.

The advantage of the EXAFS and AXS methods is that the chemical environment around a certain metallic ion in solutions can be selectively determined [15, 16]. For example, in a metal-halide aqueous solution, its total structure factor is described as the sum of ten partial structure factors, where a large contribution from the partial structure factor of O-O pairs caused by the correlation between water molecules is well-recognized. Thus, in the conventional X-ray or neutron diffraction method it is extremely hard to evaluate an environment around a metallic cation due to the lack of element selectivity. The present electroplating bath of Mo-Ni alloys is prepared by dissolving sodium molybdate, nickel sulfate and sodium

Reprint requests to K. Shinoda; Fax: 81-22-217-5211.

0932-0784 / 97 / 1200-0855 $ 06.00 © – Verlag der Zeitschrift für Naturforschung, D-72072 Tübingen

citrate with sulfuric acid to adjust the pH value to 5.0. Thus, only well-combined AXS and EXAFS methods enable us to determine the atomic structure of molybdenum and nickel complexes. In this paper we present a structural model of complexes in acid solution containing molybdenum and will discuss their change owing to the presence of nickel and citric ions by obtaining the environmental structure around molybdenum ions or nickel ions.

2. Experimental

Aqueous solutions were prepared with various concentrations of sodium molybdate dihydrate ($Na_2MoO_4 \cdot 2H_2O$), nickel sulfate hexahydrate ($NiSO_4 \cdot 6H_2O$) and sodium citrate dihydrate ($Na_3C_6H_5O_7 \cdot 2H_2O$). The pH values of these solutions were adjusted to 5.0 using dilute sulfuric acid. Aqueous solutions of 0.2 mol/l $NiSO_4$, 1.0 mol/l Na_2MoO_4, 0.5 mol/l Na_2MoO_4 + 0.5 mol/l $NiSO_4$, and 0.5 mol/l Na_2MoO_4 + 0.5 mol/l $NiSO_4$ + 1.0 mol/l Na_3 cit. were used for the EXAFS measurements. Aqueous solutions of 1.0 mol/l Na_2MoO_4, 0.5 mol/l Na_2MoO_4 + 0.5 mol/l $NiSO_4$, and 0.5 mol/l Na_2MoO_4 + 0.5 mol/l $NiSO_4$ + 1.0 mol/l Na_3 cit. were used for the AXS measurements. MoO_3 crystals were also used as a reference in the EXAFS measurement.

The EXAFS and AXS measurements were carried out at the beam line 6B in the Photon Factory (PF) of the High Energy Accelerator Research Organization (KEK), Tsukuba, Japan. Monochromatic X-ray beams are obtained using a double Si 111 crystal monochromator and monitored by an ionization chamber placed just in front of the sample. The AXS intensities were measured with a portable Ge solid state detector. The details of the experimental settings in PF are described in [17]. Some additional details required for the present work are given below. The solutions are contained in a cell with windows of a thin polymer film on both sides. The EXAFS spectra were obtained from the intensities of incident and transmitted X-ray beams measured by ionization chambers. The effect of the higher harmonics was reduced to an insignificant level by detuning the second Si crystal of the monochromator with a piezo-electric device.

The AXS intensities were collected by combining two different geometries, that is, the symmetrical transmission geometry for low scattering angles from 2° to 50° and the symmetrical reflection geometry for high scattering angles from 50° to 120°. In this way, the contribution from the cell windows is kept at low level [15]. The AXS intensities were measured on the lower energy side of the Ni and Mo K absorption edges because of particular near-edge phenomena, such as EXAFS and X-ray absorption near-edge structure (XANES), and extremely strong fluorescence radiation from the samples [18]. Empirically, two incident energies were used; that is, 8.032 and 8.132 keV below the Ni K absorption edge (8.332 keV), and 19.704 and 19.974 keV below the Mo K absorption edge (20.004 keV). The environmental structure around Ni and Mo ions was determined from the difference between the intensities at these two energies. The procedure of this AXS analysis is identical to the previous work on liquid and glass samples [15, 18]. The AXS and EXAFS methods provide us structural information around a particular element corresponding to the absorption edge [18]. The EXAFS method is especially sensitive in the first nearest neighbor pairs. On the other hand, the AXS method gives structural information for atomic pairs even at a longer distance. In the present study, we made the best use of each method. The structural parameters for adjacent Mo-O and Ni-O pairs at the first nearest neighbor distance were determined by the EXAFS method [19]. Using the structural data for Mo-O and Ni-O pairs by the EXAFS method and the differential interference functions by the AXS method [15], the structural parameters for neighboring Mo-Mo and Mo-Ni pairs at a longer distance were determined as follows.

According to Narten and Levy [20], the interference functions are given by

$$Qi(Q) = \sum_{j=1}^{n}\sum_{k=1}^{n'} c_j N_{jk} e^{-b_{jk}Q^2} \frac{f_j f_k}{\langle f\rangle^2} \frac{\sin(Qr_{jk})}{r_{jk}} + 4\pi\rho_0 \sum_{j=1}^{n}\sum_{k=1}^{n} e^{-b_{jk}Q^2} \frac{c_j c_k f_j f_k}{\langle f\rangle^2} \times \frac{QR_{jk}\cos(QR_{jk}) - \sin(QR_{jk})}{Q^2}, \quad (1)$$

where $Q = 4\pi \sin\theta/\lambda$. Further, n is the number of elements, n' the number of j-k pairs taken into account in the calculation, N_{jk} the coordination number of j-k pairs at the distance r_jk, and b_{jk} the mean squares variation. The quantities R_{jk} and B_{jk} represent the mean and variance of the boundary region which need not to be sharp. In practice, the distance and coordination numbers of near neighbor pairs are obtained by

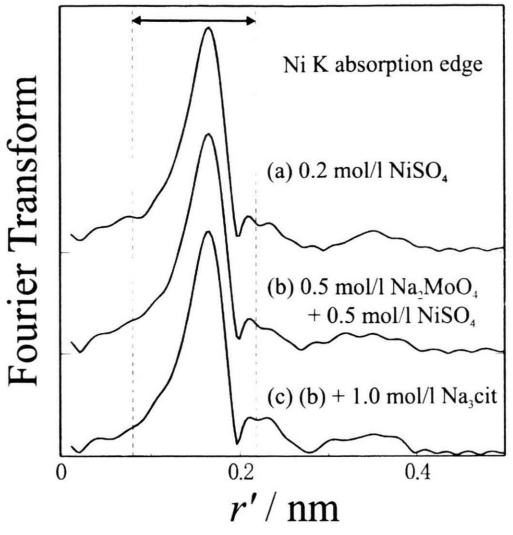

Fig. 1. Fourier transforms of weighted EXAFS spectra in (a) 0.2 mol/l $NiSO_4$, (b) 0.5 mol/l Na_2MoO_4 + 0.5 mol/l $NiSO_4$, and (c) 0.5 mol/l Na_2MoO_4 + 0.5 mol/l $NiSO_4$ + 1.0 mol/l Na_3 cit. aqueous solutions.

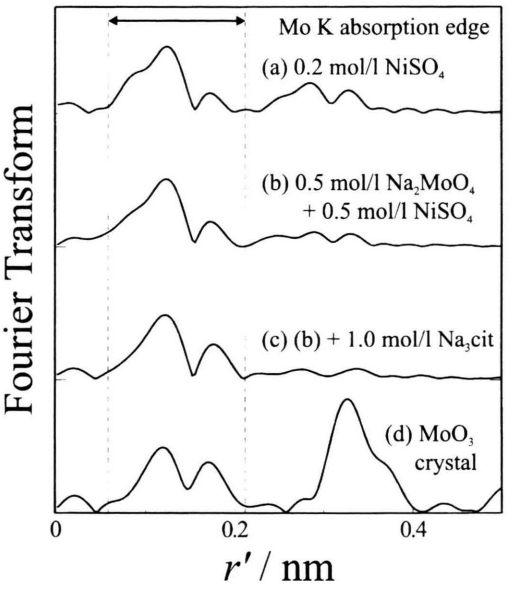

Fig. 2. Fourier transforms of weighted EXAFS spectra in (a) 1.0 mol/l Na_2MoO_4, (b) 0.5 mol/l Na_2MoO_4 + 0.5 mol/l $NiSO_4$, and (c) 0.5 mol/l Na_2MoO_4 + 0.5 mol/l $NiSO_4$ + 1.0 mol/l Na_3 cit. aqueous solutions, and (d) MoO_3 crystal.

the least-squares calculation of (1) so as to reproduce the experimental interference function [20, 21]. The differential interference function by the AXS method is readily calculated by taking the difference between two interference functions in (1), evaluated at the two energies below the absorption edge [22].

Small-angle X-ray scattering (SAXS) measurements were also carried out in transmission geometry with monochromatic MoKα_1 radiation by a Ge 220 channel-cut monochromator. A rotating X-ray generator, operated at 54 kV and 280 mA, was used. The SAXS intensity from the aqueous solutions filled in a glass capillary tube of 2mm diameter was detected with a xenon-filled one-dimensional position sensitive proportional counter. The beam path, 480 mm long from sample to detector, was evacuated. The SAXS intensity, observed from 0.5 to 16 nm^{-1}, was corrected for background intensity, absorption and multiple scattering and converted to absolute units using a scaling factor determined by comparing the theoretical value with the value at Q = 0, extrapolated from the experimental intensity data of pure water [23].

3. Results

The radial structure function (RSF) in the distance r' space is obtained by Fourier transform of the weighted EXAFS spectra $k^3\chi(k)$ in momentum k space [19]. Here r' is related to the true distance r by a phase shift. The RSFs for Ni ions in 0.2 mol/l $NiSO_4$, 0.5 mol/l Na_2MoO_4 + 0.5 mol/l $NiSO_4$, and 0.5 mol/l Na_2MoO_4 + 0.5 mol/l $NiSO_4$ + 1.0 mol/l Na_3 cit. aqueous solutions are shown in Figure 1. The first peaks in Fig. 1 show no significant difference in these solutions. Similarly, the RSFs for Mo ions obtained at the MoK absorption edge in 1.0 mol/l Na_2MoO_4, 0.5 mol/l Na_2MoO_4 + 0.5 mol/l $NiSO_4$, and 0.5 mol/l Na_2MoO_4 + 0.5 mol/l $NiSO_4$ + 1.0 mol/l Na_3 cit. aqueous solutions are shown in Figure 2. The first peaks at about 0.12 and 0.18 nm in Fig. 2(a) to (c) also show no significant difference in all solutions. Thus, these Ni and Mo RSFs indicate that the first shells around Ni and Mo ions are not influenced by a species of ions in solution.

Coordination numbers and atomic distances for the first shell around Ni ions were determined by the Fourier-filtering method. The region between the dotted lines in Fig. 1 indicates the width of the window function used to filter the first neighboring shell. The Fourier-filtered Ni EXAFS spectra $k^3\chi(k)$ are shown with solid curves in Figure 3. The dashed curves in Fig. 3 correspond to those calculated by the structural parameters in Table 1. In similar way, the coor-

Table 1. Coordination numbers and atomic distances in the first shell determined from the Ni EXAFS spectra in 0.2 mol/l $NiSO_4$, 0.5 mol/l Na_2MoO_4 + 0.5 mol/l $NiSO_4$, and 0.5 mol/l Na_2MoO_4 + 0.5 mol/l $NiSO_4$ + 1.0 mol/l Na_3 cit. aqueous solutions. Their experimental errors are ±0.2 and ±0.001 nm, respectively.

Aqueous solution	Ni–O pair	
	r / nm	N
0.2 mol/l $NiSO_4$	0.205	6.0
0.5 mol/l Na_2MoO_4 + 0.5 mol/l $NiSO_4$	0.205	6.0
0.5 mol/l Na_2MoO_4 + 0.5 mol/l $NiSO_4$ + 1.0 mol/l Na_3 cit.	0.205	6.0

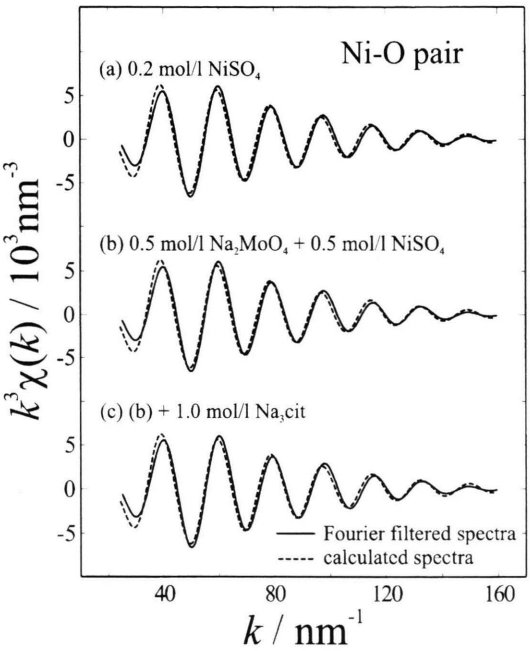

Fig. 3. Fourier-filtered Ni EXAFS spectra in (a) 0.2 mol/l $NiSO_4$, (b) 0.5 mol/l Na_2MoO_4 + 0.5 mol/l $NiSO_4$, and (c) 0.5 mol/l Na_2MoO_4 + 0.5 mol/l $NiSO_4$ + 1.0 mol/l Na_3 cit. aqueous solutions.

Table 2. Coordination numbers and atomic distances in the first shell determined from the Mo EXAFS spectra in 1.0 mol/l Na_2MoO_4, 0.5 mol/l Na_2MoO_4 + 0.5 mol/l $NiSO_4$, and 0.5 mol/l Na_2MoO_4 + 0.5 mol/l $NiSO_4$ + 1.0 mol/l Na_3 cit. aqueous solutions, and MoO_3 crystal. Their experimental errors are ±0.2 and ±0.001 nm, respectively.

Aqueous solution	Mo-O(1)		Mo-O(2)		Mo-O(3)	
	r / nm	N	r / nm	N	r / nm	N
1.0 mol/l Na_2MoO_4	0.173	2.1	0.193	2.0	0.224	2.0
0.5 mol/l Na_2MoO_4 + 0.5 mol/l $NiSO_4$	0.172	2.1	0.192	2.2	0.223	1.9
0.5 mol/l Na_2MoO_4 + 0.5 mol/l $NiSO_4$ + 1.0 mol/l Na_3 cit.	0.172	2.0	0.194	2.1	0.228	2.0
MoO_3	0.170	2.0	0.194	2.0	0.229	2.0

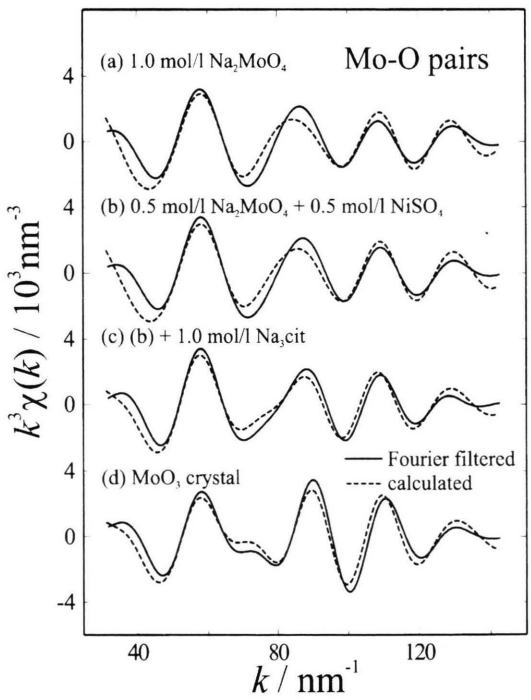

Fig. 4. Fourier-filtered Mo EXAFS spectra in (a) 1.0 mol/l Na_2MoO_4, (b) 0.5 mol/l Na_2MoO_4 + 0.5 mol/l $NiSO_4$, and (c) 0.5 mol/l Na_2MoO_4 + 0.5 mol/l $NiSO_4$ + 1.0 mol/l Na_3 cit. aqueous solutions, and (d) a MoO_3 crystal.

dination numbers and atomic distances for the first shell around Mo ions were also determined using the Fourier-filtered Mo EXAFS spectra in Figure 4. The Ni EXAFS spectra in Fig. 3 are found to be well explained by a single Ni-O distance model (cf. Table 1). On the other hand, three Mo-O pairs with different distances are required to fully fit the Mo EXAFS spectra in Figure 4. This is verified by the EXAFS spectrum of the MoO_3 crystal in Figure 4(d). According to the structural data of crystalline MoO_3 [24], the structural unit is a distorted octahedron consisting of a molybdenum atom surrounded by 6 oxygen atoms. These 6 oxygen atoms are grouped in pairs by 3 different Mo-O distances of 0.167 - 0.173, 0.195 and 0.225 - 0.233 nm. These values are consistent with the present EXAFS results in MoO_3 crystal summarized in Table 2. Consequently, the Mo EXAFS spectra of solutions in Fig. 4 were also analyzed with the

Table 3. Coordination numbers and atomic distances of Mo-Mo and/or Mo-Ni pairs in 1.0 mol/l Na_2MoO_4, 0.5 mol/l Na_2MoO_4 + 0.5 mol/l $NiSO_4$, and 0.5 mol/l Na_2MoO_4 + 0.5 mol/l $NiSO_4$ + 1.0 mol/l Na_3 cit. aqueous solutions. Their experimental errors are ±0.2 and ±0.002 nm, respectively. Coordination numbers and atomic distances of Mo-Mo and Mo-Ni pairs in $Na_6Mo_7O_{24}\cdot 14H_2O$ [25] and $Na_3(CrMo_6O_{24}H_6)\cdot 8H_2O$ [28] crystals are calculated from the crystalline data.

Sample	Mo-Mo		Mo-Ni	
	r / nm	*N*	*r* / nm	*N*
1.0 mol/l Na_2MoO_4 sol.	0.335	2.9	–	–
0.5 mol/l Na_2MoO_4 + 0.5 mol/l $NiSO_4$ sol.	0.329	2.1	0.331	1.3
$Na_6Mo_7O_{24}\cdot 14H_2O$ crystal	0.333	3.1	–	–
$Na_3(CrMo_6O_{24}H_6)\cdot 8H_2O$ crystal	0.333	2.0	0.333	1.0

	Mo-Mo(Ni)	
	r / nm	*N*
0.5 mol/l Na_2MoO_4 + 0.5 mol/l $NiSO_4$ + 1.0 mol/l Na_3 cit. sol.	0.331	1.4

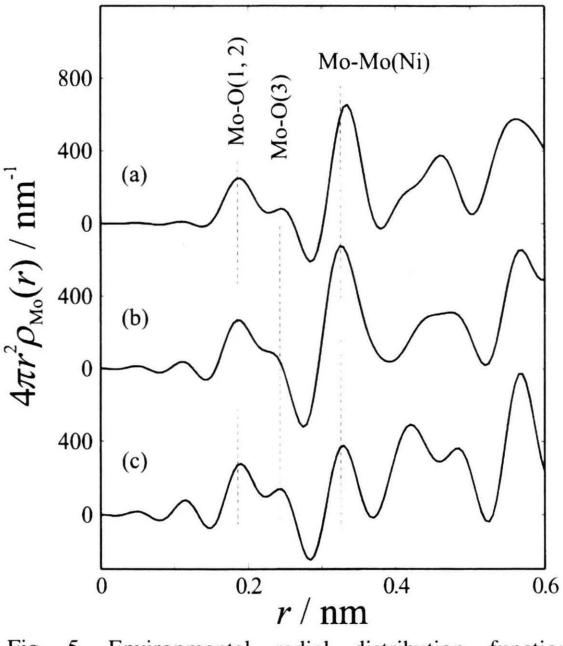

Fig. 5. Environmental radial distribution functions around Mo ions, $4\pi r^2\rho_{Mo}(r)$, in (a) 1.0 mol/l Na_2MoO_4, (b) 0.5 mol/l Na_2MoO_4 + 0.5 mol/l $NiSO_4$, and (c) 0.5 mol/l Na_2MoO_4 + 0.5 mol/l $NiSO_4$ + 1.0 mol/l Na_3 cit. aqueous solutions.

model of three Mo-O distances as given in Table 2. This clearly indicates that the Mo ions form distorted MoO_6 octahedra even in the solutions.

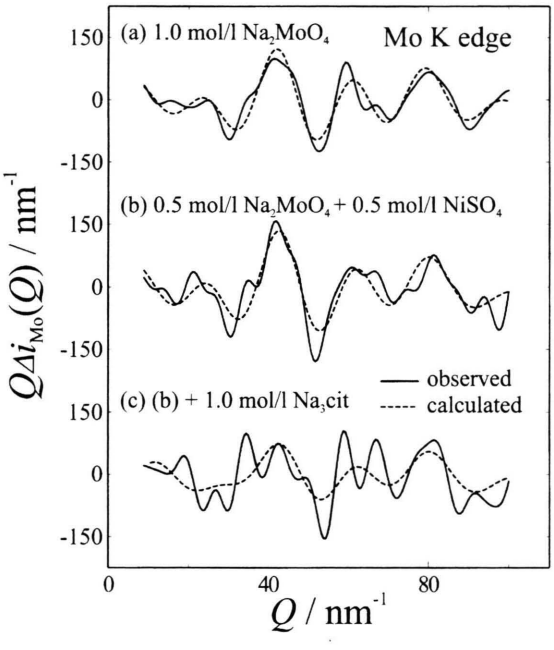

Fig. 6. Differential interference functions $Q\Delta i_{Mo}(Q)$ of (a) 1.0 mol/l Na_2MoO_4, (b) 0.5 mol/l Na_2MoO_4 + 0.5 mol/l $NiSO_4$, and (c) 0.5 mol/l Na_2MoO_4 + 0.5 mol/l $NiSO_4$ + 1.0 mol/l Na_3 cit. aqueous solutions determined by the AXS method at Mo K absorption edge.

Figure 5 shows the environmental radial distribution functions (RDFs) for Mo ions determined by the AXS method in 1.0 mol/l Na_2MoO_4, 0.5 mol/l Na_2MoO_4 + 0.5 mol/l $NiSO_4$, and 0.5 mol/l Na_2MoO_4 + 0.5 mol/l $NiSO_4$ + 1.0 mol/l Na_3 cit. aqueous solutions. From the structural data of the nearest neighbor Mo-O pairs in Table 2, we find that the two peaks at about 0.18 and 0.23 nm in the RDFs in Fig. 5 can be attributed to the overlapped Mo-O(1) and Mo-O(2) pairs, and the Mo-O(3) pairs, respectively. As seen in Fig. 2, any appreciable peak at about 0.33 - 0.34 nm is absent in the Fourier transform of weighted EXAFS spectra of solutions. Whereas an apparent peak of Mo-Mo pairs, indicating an edge sharing linkage between MoO_6 octahedra, is observed in the MoO_3 crystal. Quantitative analyses of Mo-Mo(Ni) pairs in solutions are known to be very difficult from the EXAFS data alone. On the other hand, distinct peaks of Mo-Mo(Ni) pairs are observed at about 0.33 nm in the environmental RDFs for Mo in Figure 5. Thus, the structural parameters for Mo-Mo(Ni) pairs in solutions were accurately estimated from the AXS data at the MoK absorption edge. In combination with the structural parameters for the Mo-O pairs in Table 2, and the

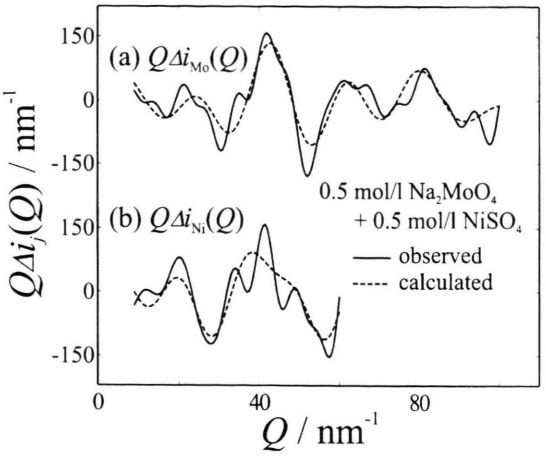

Fig. 7. Differential interference functions for (a) Mo and (b) Ni in 0.5 mol/l Na_2MoO_4 + 0.5 mol/l $NiSO_4$ aqueous solution determined by the AXS measurements at Mo and Ni K absorption edges.

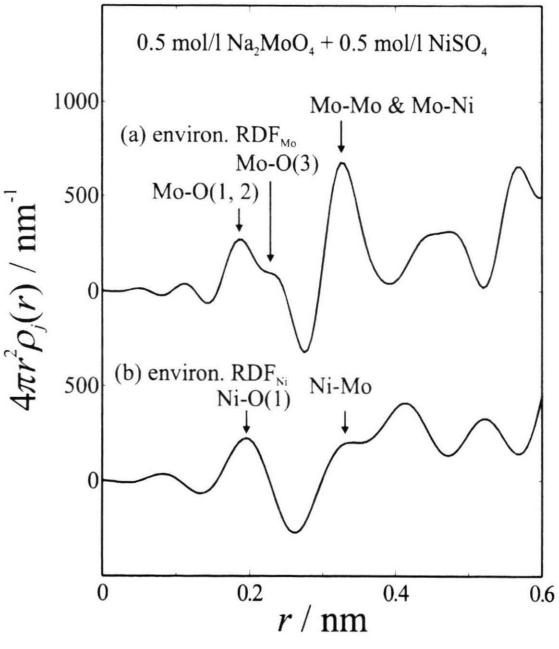

Fig. 8. Environmental radial distribution functions around (a) Mo and (b) Ni ions in 0.5 mol/l Na_2MoO_4 + 0.5 mol/l $NiSO_4$ aqueous solution.

differential interference functions for Mo, $Q\Delta i_{Mo}(Q)$ obtained from the AXS measurements at the MoK absorption edge in Fig. 6, the coordination numbers and atomic distances at about 0.33 nm were determined by the least squares variational method. The strcutural parameters for Mo-Mo and Mo-Ni pairs are summarized in Table 3.

In the 0.5 mol/l Na_2MoO_4 + 0.5 mol/l $NiSO_4$ aqueous solution, the structural parameters of Mo-Mo and Mo-Ni were independently determined by fitting the two differential interference functions for Mo and Ni in Figure 7. As shown in Fig. 8, we can find the peaks at about 0.33 nm in both environmental RDFs for Mo and Ni obtained by Fourier transform of the differential interference functions. The peak at about 0.33 nm in the environmental RDF for Mo in Fig. 8(a) is attributed to Mo-Mo and Mo-Ni pairs. Thus, by combining the structural parameters for the Ni-O pairs in Table 1 with the function $Q\Delta i_{Ni}(Q)$ in Fig. 7(b), we could first determine the structural data for Ni-Mo pairs. Next, by applying these Ni-Mo data as well as the Mo-O data in Table 2 to the function $Q\Delta i_{Mo}(Q)$ in Fig. 7(a), we finally obtained the structural data for Mo-Mo and Mo-Ni pairs summarized in Table 3.

4. Discussion

According to the structural data in Table 2, the structural unit in the 1.0 mol/l Na_2MoO_4 solution is considered to be a distorted MoO_6 octahedron which is similar to the one in the MoO_3 crystal. Since the atomic distance of Mo-Mo pairs in the Na_2MoO_4 solution is 0.335 nm in Table 3, the MoO_6 octahedra are likely to be connected by sharing their edges. Because of the coincidence between the data of Mo-Mo pairs in the Na_2MoO_4 solution and the crystalline $Na_6Mo_7O_{24}\cdot 14H_2O$ data [25], it is likely that the local ordering of the MoO_6 octahedra is very close to the cluster in the crystal. Accordingly, molybdenum ions in the 1.0 mol/l Na_2MoO_4 solution form poly-molybdate ions as illustrated in Figure 9(a). Such poly-molybdate ions consist of 7 MoO_6 octahedra which are connected by sharing their edges. This is

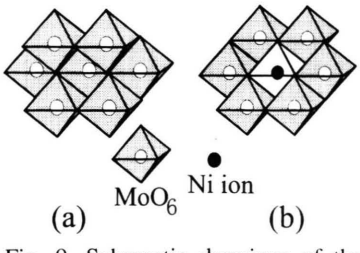

Fig. 9. Schematic drawings of the structural models of poly-molybdate in (a) 1.0 mol/l Na_2MoO_4, and (b) 0.5 mol/l Na_2MoO_4 + 0.5 mol/l $NiSO_4$ aqueous solutions.

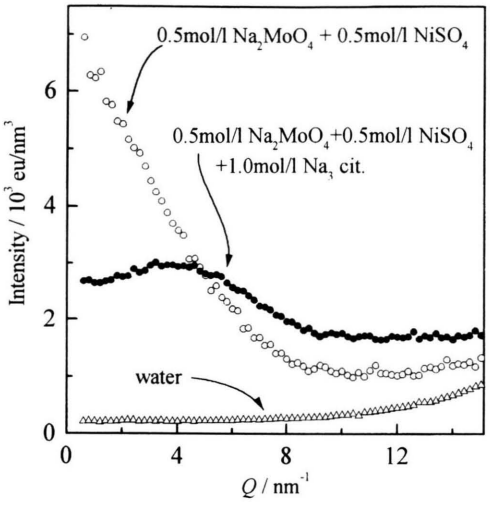

Fig. 10. Small angle X-ray scattering intensity profiles of 0.5 mol/l Na_2MoO_4 + 0.5 mol/l $NiSO_4$ (open circles) and 0.5 mol/l Na_2MoO_4 + 0.5 mol/l $NiSO_4$ + 1.0 mol/l Na_3 cit. (solid circles) aqueous solutions, and pure water (open triangles).

consistent with the fact [26, 27] that molybdenum ions form mainly $Mo_7O_{24}^{6-}$ oxo-complexes consisting of 7 MoO_6 octahedra in an acid molybdate aqueous solution.

The structural unit of the MoO_6 octahedron does not change in the presence of Ni ions, as it is clearly seen in Table 2. Table 3 shows that the coordination numbers and atomic distances of Mo-Mo and Mo-Ni pairs in the 0.5 mol/l Na_2MoO_4 + 0.5 mol/l $NiSO_4$ solution agree well with the values of the $Na_3(CrMo_6O_{24}H_6)\cdot 8H_2O$ crystal [28]. Thus, it is plausible that all Mo ions and a part of the Ni ions form the poly-molybdate ion shown in Fig. 9(b) which is the cluster in the $Na_3(CrMo_6O_{24}H_6)\cdot 8H_2O$ crystal in spite of the difference between Ni and Cr. This result is confirmed by the fact that the $Na_3(CrMo_6O_{24}H_6)\cdot 8H_2O$ single crystal was grown from an aqueous solution containing Na_2MoO_4 and $Cr(NO_3)_3$ at a 6 to 1 ratio with pH of 4.5 [28].

We notice in Fig. 5 that the peak height due to Mo-Mo(Ni) pairs at about 0.33 nm is reduced in the solution containing citric ions. Although the total number of Mo and Ni around Mo at 0.33 nm is 3.4 in the 0.5 mol/l Na_2MoO_4 + 0.5 mol/l $NiSO_4$ solution, it becomes 1.4 when adding 1.0 mol/l Na_3 citrate to the solution. Figure 10 shows the SAXS intensities observed in the 0.5 mol/l Na_2MoO_4 + 0.5 mol/l $NiSO_4$ and 0.5 mol/l Na_2MoO_4 + 0.5 mol/l $NiSO_4$ + 1.0 mol/l Na_3 cit. aqueous solutions. The SAXS intensity in the low Q-region decreases by adding citric ions to the 0.5 mol/l Na_2MoO_4 + 0.5 mol/l $NiSO_4$ solution. This implies that relatively larger clusters are likely to be present in the 0.5 mol/l Na_2MoO_4 + 0.5 mol/l $NiSO_4$ solution, whereas only small ones are in the 0.5 mol/l Na_2MoO_4 + 0.5 mol/l $NiSO_4$ + 1.0 mol/l Na_3 cit. solution. Taking account of this SAXS observation in Fig. 10 and the decrease in the total coordination numbers around Mo in Table 3, it may safely be said that the large poly-molybdate ions in Fig. 9(b) are decomposed into small molybdate ions consisting of at most a few MoO_6 octahedra when adding citric ions to the 0.5 mol/l Na_2MoO_4 + 0.5 mol/l $NiSO_4$ solution. The mechanism of this decomposition process can probably be explained in the following way. The nickel ion is located in the center of the poly-molybdate ion in Figure 9(b). Such nickel ions form citric complexes. Thus, Mo and Ni ions cannot form the large poly-molybdate ions any longer. According to our recent measurements of visible absorption spectra of the present aqueous solution, the small poly-molybdate ions as well as Ni ions are found to form citric complexes [29].

Molybdenum is only electrodeposited from a solution containing Mo, Ni and citric ions [30]. In such a solution, molybdenum ions exist as small molybdate ions which probably form citric complexes. Consequently, we consider that these small Mo(VI)-citrate complexes play an important role in the mechanism of the induced codeposition.

5. Summary

The environment around molybdenum and nickel ions in 1.0 mol/l Na_2MoO_4, 0.5 mol/l Na_2MoO_4 + 0.5 mol/l $NiSO_4$, and 0.5 mol/l Na_2MoO_4 + 0.5 mol/l $NiSO_4$ + 1.0 mol/l Na_3 cit. aqueous solutions at pH = 5.0 has been determined by skillfully combining the AXS and EXAFS methods. In the 1.0 mol/l Na_2MoO_4 solution, molybdenum ions form relatively large poly-molybdate ions consisting of 7 MoO_6 octahedra. In the 0.5 mol/l Na_2MoO_4 + 0.5 mol/l $NiSO_4$ solution, molybdenum ions form poly-molybdate ions consisting of 6 MoO_6 octahedra surrounding an Ni ion. By adding 1.0 mol/l Na_3 citrate to the 0.5 mol/l Na_2MoO_4 + 0.5 mol/l $NiSO_4$ solution, these relatively large complexes are decomposed to small Mo(VI)-citrate complexes. This structural change of the molybdate ions in the solution is considered to be an important factor controlling the mechanism of induced codeposition.

Acknowledgements

This research was supported by Grant-in-Aid for Scientific Research, the Ministry of Education, Science and Culture (No. 09212216 and No. 09305052). We particularly thank the staff in the Photon Factory, High Energy Accelerator Research Organization, Professor M. Nomura and Dr. A. Koyama. One of the authors (KS) is also grateful to the Japan Society for the Promotion of Science for Research Fellowships.

[1] V. Q. Kinh, E. Chassaing, and M. Saurat, Electrodep. Surf. Treat. **3**, 205 (1975).
[2] K. WiKeil and J. Osteryoung, J. Appl. Electrochem. **22**, 506 (1992).
[3] I. A. Raj, J. Mat. Sci., 28, 4375 (1993).
[4] A. Brenner, Electrodeposition of Alloys **2**, Chapt. 34, Academic Press Inc., New York 1963.
[5] D. W. Ernst and M. L. Holt, J. Electrochem. Soc. **105**, 686 (1958).
[6] S. Rengakuji, Y. Nakamura, M. Inoue, K. Nishibe, and H. Imanaga, Denki Kagaku **59**, 885 (1991).
[7] H. Fukushima, T. Akiyama, S. Akagi, and K. Higashi, Trans. Japan Inst. Metals **20**, 358 (1979).
[8] E. J. Podlaha, M. Matlosz, and D. Landolt, J. Electrochem. Soc., **140**, L149 (1993).
[9] E. J. Podlaha and D. Landolt, J. Electrochem. Soc. **143**, 885 (1996).
[10] K. Higashi and H. Fukushima, J. Metal Finish. Soc. Japan **24**, 486 (1973).
[11] C. C. Nee, W. Kim, and R. Weil, J. Electrochem. Soc. **135**, 1100 (1988).
[12] B. Yuan, K. Liu, and M. Kowaka, J. Finish. Soc. Japan **42**, 639 (1991).
[13] S. Yao and M. Kowaka, J. Metal Finish. Soc. Japan **39**, 736 (1988).
[14] T. Akiyama, H. Fukushima, F. Yuse, T. Tsuru, and Y. Tomokiyo, J. Finish. Soc. Japan **46**, 1133 (1995).
[15] E. Matsubara and Y. Waseda, J. Phys.: Condens. Matter **1**, 8575 (1989).
[16] E. Matsubara, K. Okuda, and Y. Waseda, J. Phys.: Condens. Matter, **2**, 9133 (1990).
[17] E. Matsubara, K. Harada, Y. Waseda, and M. Iwase, Z. Naturforsch., **43a**, 181 (1988).
[18] Y. Waseda, Novel Application of Anomalous X-ray Scattering for Structural Characterization of Disordered Materials, Springer, New York 1984.
[19] For example, B. K. Teo, EXAFS: Basic Principles and Data Analysis, Springer, New York 1986.
[20] A. H. Narten and H. A. Levy, Science **160**, 447 (1969).
[21] A.H.Narten, J. Chem. Phys. **56**, 1905 (1972).
[22] E. Matsubara, K. Sugiyama, Y. Waseda, M. Ashizuka, and E. Ishida, J. Mat. Sci. Let. **9**, 14 (1990).
[23] H. Hayashi, K. Nishikawa, and T. Iijima, Japan J. Appl. Phys. **28**, 1501(1989)
[24] L. Kihlborg, Arkiv för Kemi **21**, 357, (1963).
[25] K. Sjobom and B. Hedman, Acta Chem. Scand. **27**, 3673 (1973).
[26] F. A. Cotton and G. Wilkinson, Advanced Inorganic Chemistry, 5th ed., Interscience-Wiley, New York 1988, p.817.
[27] G. Johansson, L. Pettersson, and N. Ingri, Acta Chem. Scand. **A28**, 1119 (1974).
[28] A. Perloff, Inorg. Chem. **9**, 2228 (1970).
[29] E. Uekawa, K.Murase, E.Matsubara, T.Hirato, and Y.Awakura, J. Electrochem. Soc., to be published.
[30] T. Watanabe, T. Naoe, A. Mitsuo, and S. Katsumata, J. Finish. Soc. Japan **40**, 458 (1989).